Computational Pollutant Environment Assessment from Propulsion-System Testing

Ten-See Wang, Paul McConnaughey,
Yen-Sen Chen, Saif Warsi

Reprinted from

Journal of Spacecraft and Rockets

Volume 33, Number 3, Pages 386–392

AIAA

A publication of the
American Institute of Aeronautics and Astronautics, Inc.
1801 Alexander Bell Drive, Suite 500
Reston, VA 22091

JOURNAL OF SPACECRAFT AND ROCKETS
Vol. 33, No. 3, May–June 1996

Computational Pollutant Environment Assessment from Propulsion-System Testing

Ten-See Wang* and Paul McConnaughey†
NASA Marshall Space Flight Center, Huntsville, Alabama 35812
Yen-Sen Chen‡
Engineering Sciences, Inc., Huntsville, Alabama 35805
and
Saif Warsi§
Sverdrup Technology, Inc., Huntsville, Alabama 35806

An asymptotic plume growth method based on a time-accurate three-dimensional computational fluid dynamics formulation has been developed to assess the exhaust-plume pollutant environment from a simulated RD-170 engine hot-fire test on the F1 Test Stand at Marshall Space Flight Center. Researchers have long known that rocket-engine hot firing has the potential for forming thermal nitric oxides, as well as producing carbon monoxide when hydrocarbon fuels are used. Because of the complex physics involved, most attempts to predict the pollutant emissions from ground-based engine testing have used simplified methods, which may grossly underpredict and/or overpredict the pollutant formations in a test environment. The objective of this work has been to develop a computational fluid dynamics-based methodology that replicates the underlying test-stand flow physics to accurately and efficiently assesses pollutant emissions from ground-based rocket-engine testing. A nominal RD-170 engine hot-fire test was computed, and pertinent test-stand flow physics was captured. The predicted total emission rates compared reasonably well with those of the existing hydrocarbon engine hot-firing test data.

Nomenclature

C_1, C_2, C_3	= turbulence modeling constants = 1.15, 1.9, and 0.25, respectively
F	= convection and diffusion fluxes
G	= turbulent kinetic energy production
H	= enthalpy
J	= Jacobian of coordinate transformation
K_f	= Arrhenius forward reaction rate constant
k	= turbulent kinetic energy
N	= total number of species
p	= static pressure
Q	= heat source
q	= $l, u, v, w, H, k, \varepsilon$, or α_i
R_q	= residue term for q equation
S_q	= source term for q equation
T	= static temperature
U	= transformed velocity, (contravariant velocity) × volume
u, v, w	= mean velocities in x, y, and z directions
x, y, z	= physical coordinates
α_i	= mass fraction for species i
Δq	= difference operator, $\Delta q_{i+1/2} = q_{i+1} - q_i$
ε	= turbulent kinetic energy dissipation rate
μ_e	= effective viscosity
μ_t	= turbulent eddy viscosity
ξ	= computational coordinates
ρ	= density
Φ	= energy dissipation function, ρG
ω_i	= mass production rate for species i

Received April 4, 1995; revision received Dec. 11, 1995; accepted for publication Dec. 13, 1995.

*Team Leader, Computational Analysis Team. Member AIAA.
†Branch Chief, Fluid Dynamics Analysis Branch. Member AIAA.
‡President. Member AIAA.
§Aerospace Engineer. Member AIAA.

Introduction

RUSSIAN-BUILT kerosene-fueled engines such as the RD-170 and the U.S. counterpart RD-704 have been identified as potential candidates to power single-stage-to-orbit rockets. The potential for formation of thermal nitric oxides (NO_x) and carbon monoxide (CO) is a concern during ground-based testing of rocket engines that use hydrocarbon fuels. The release of NO_x into the atmosphere contributes to acid rain and ozone depletion, and the CO poses a potential threat to living organisms. Since an environmental impact assessment is required before testing can begin, it is important to accurately assess the potential pollutant levels. Several simplified analyses have been used in the past for first-order estimates. For example, thermochemical analysis using the chemical equilibrium computer code[1] can provide CO concentration estimates at the nozzle exit plane. However, the nozzle exit solution overpredicts the CO concentration because it does not include the subsequent afterburning with air. Additionally, it cannot predict NO_x formation unless the correct amount of air mixing is assumed. A perfectly stirred-reactor analysis has been reported to treat the plume–air mixing.[2] While attractive because of its simplicity, the assumption of perfect mixing between the plume and entrained air is not justified. Also, there is an inherent difficulty in estimating the residence time. Other methods, such as steady two-dimensional analysis of a free-exhaust plume, can be used; however, the physics depicted does not adequately replicate the complex three-dimensional transient phenomena that occur during the engine testing. A variational-principle-based computational fluid dynamics (CFD) method was used to perform a two-dimensional transient analysis[3] of the Space Shuttle main-engine exhaust in a covered flame trench. The focus, however, was not the evaluation of the pollutant environment but the assessment of the potential for a hazardous engine cutoff.

The rapid gains made in CFD and computer technologies have made possible the development of a computational methodology that can describe the complex pollutant emission physics resulting from ground-based rocket-engine tests. These physical processes include three-dimensional air entrainment, three-dimensional multiple-nozzle plume interaction and mixing with air, finite-rate plume afterburning, plume impingement with the ski slope of the flame bucket and quenching through deluge water, and

three-dimensional restricted multiple-plume expansion. To simulate an actual hot firing, however, is still cost-prohibitive, because actual hot firing on a test stand is a three-dimensional transient phenomenon. An asymptotic plume growth method is developed in this study in which a steady–transient process is described instead of the actual startup and cutoff sequences. From an environmental assessment viewpoint, the emission rate obtained from a steady–transient process is preferred, since it is usually conservative if full power level is simulated. Other issues aside, even if limited emission data were available, benchmarking of the CFD model with actual hot firings is impractical from a time–cost standpoint. Past hot firings were usually not useful for CFD benchmarking, since not all of the boundary conditions were or can be measured. Accordingly, the most efficient strategy is to base the methodology on numerical models and submodels that have been previously benchmarked with simpler, but still relevant aspects pertaining to test-stand flow physics. Importantly, with the emphasis on computational tractability,[4] the models and submodels used should not be so computationally intensive as to preclude use in three-dimensional applications. Following that strategy, a pressure-based CFD method was chosen as the basic CFD formulation. Combustion-driven flows relevant to this problem for which the methodology has been benchmarked include a dump combustor[5] and rocket-engine combustors,[6] unified combustor–nozzle–plume flowfields,[7] transient flows in a rocket-engine combustor[8] during startup, transient flow separation inside the thrust chamber and transient plume development during both startup and cutoff,[9] and three-dimensional base flowfields for a four-engine clustered nozzle configuration[10] similar to the four-nozzle cluster setup of the RD-170. The turbulence and chemistry submodels were chosen with efficiency in mind. The specific rationale for those submodels chosen and the pertinent benchmarks performed are detailed in the later sections. The hot firing of an RD-170 engine on the F1 Test Stand at NASA Marshall Space Flight Center (MSFC) was simulated numerically. A nominal hot firing with water quenching was computed. Two parallel cases using the frozen chemistry and finite-rate chemistry, but without water quenching, were also computed for comparison. The emission rates of the pollutants and the exhaust-plume properties were computed, and the effects of afterburning and water quenching on pollutant formation were compared. In addition to ground testing, this resultant technology has potential applications in actual rocket launches and in the development of air-breathing engines.

Asymptotic Plume Growth Method

To assess the pollutant environment from RD-170 propulsion system testing, an asymptotic plume growth method is proposed, based on the recognition that the expansion of a rocket plume during a continuous hot firing is a transient process.[3,9] That is, the plume boundary based on species concentration continues to grow with time. However, some of the plume properties near the nozzle exit plane (Mach number, for example) approximate a fixed pattern during the entire steady firing. Even after the engine is shut off, the heated plume will continue to rise and expand because of buoyancy forces. Wind direction and strength also influence the plume growth. A significant amount of the pollutant mass, if not the entire amount, is generated during the steady hot firing at the full power level. The total mass of the pollutants will not change significantly with the engine cutoff and the subsequent rapid plume quenching, but dispersion into the surrounding atmosphere does occur. Furthermore, the pollutant emission rates, as well as the plume volume growth rate, should reach an asymptotic state during a steady hot firing. The asymptotic plume growth method therefore assumes that the total mass of the pollutants can be obtained by calculating their total emission rates through a time-accurate CFD computation as the plume growth solution reaches its asymptotic state. In this study, an asymptotic state of plume growth is reached when the rate of plume volume growth and the rates of species emission converge to approximate constant levels, and the outer plume boundary is defined at a CO_2 mass fraction of 0.01%.

A weakness of the conventional point sampling technique practiced in test measurements and steady two-dimensional analyses is that data are taken at certain locations of the plume and the total mass of the pollutant of the entire plume is inferred. The proposed method integrates the total mass of pollutant from every computational cell inside the plume boundary, thus accounting for all of the pollutant mass from the entire plume. The computation is started by performing a frozen-chemistry analysis for a short period of elapsed time to establish an initial plume in the system. This process not only yields an initial flowfield for the computation of subsequent parallel finite-rate chemistry and nominal (finite-rate chemistry with water quenching) cases, but also serves as an excellent check of mass conservation using an elemental carbon balance. This procedure is acceptable because it is the total pollutant emission rates during a nominal steady RD-170 hot-firing that are desired and not those of actual startup and shutdown sequences.[9]

The goals were therefore to compute the growth rate of NO and the disappearance rate of CO until they achieve asymptotic states. A time-accurate computation is conducted until the asymptotic emission rates are obtained. Thus, a conservative prediction (full power level) of the total pollutant emissions can be achieved without having to compute through the entire test time. In this case, the emission rates obtained from a computational elapsed time of 0.1 s can be used to predict the total pollutant emissions for a 200-s (or more) steady hot-fire test. Since the real time is taken out of the computation, the proposed method is efficient for any test duration.

Governing Equations

The finite difference Navier–Stokes code[7,11,12] was used to provide multicomponent, transient viscous flowfield solutions by solving the Reynolds-averaged transport equations including mass conservation equation, momentum equations, energy equation, and other scalar transport equations. The general form of these conservation equations can be written as

$$\frac{\partial \rho q}{\partial t} + \frac{\partial}{\partial x_j}\left(\rho u_j q - \mu_e \frac{\partial q}{\partial x_j}\right) = S_q \tag{1}$$

The source terms for the governing equations in a three-dimensional space x_i can be written in fully conservative form as

$$S_q = \begin{Bmatrix} 0 \\ -\dfrac{\partial p}{\partial x_i} + \dfrac{\partial}{\partial x_j}\left(\mu_e \dfrac{\partial u_j}{\partial x_i}\right) - \dfrac{2}{3}\dfrac{\partial}{\partial x_i}\left(\mu_e \dfrac{\partial u_j}{\partial x_j}\right) \\ (Dp/Dt) + \Phi + Q \\ \rho(G - \varepsilon) \\ \rho(\varepsilon/k)\{[C_1 + C_3(G/\varepsilon)]G - C_2\varepsilon\} \\ \omega_i, \quad i = 1, \ldots, N \end{Bmatrix} \tag{2}$$

where

$$G = \frac{\mu_t}{\rho}\left\{\frac{1}{2}\left(\frac{\partial u_j}{\partial x_i} + \frac{\partial u_i}{\partial x_j}\right)^2 - \frac{2}{3}\left(\frac{\partial u_k}{\partial x_k}\right)^2\right\} \tag{3}$$

An extended k–ε turbulence model[13] is used to describe the turbulence. It is superior to the standard k–ε model[14] for flows containing shear layers where the mean strain rate is high. A second time scale of the production range of the turbulence kinetic energy spectrum is added to the dissipation rate equation and allows the energy transfer mechanism of the turbulence model to respond to the mean strain more effectively. Furthermore, that extra term represents the energy transfer rate from large-scale turbulence (low wave number) to small-scale turbulence (high wave number) controlled by the production-range time scale and the dissipation-rate time scale. Hence, albeit a single-spectrum formulation, the extended k–ε model gives performance somewhat analogous to that of the multiple-scale model[15] in which a transfer of energy from the larger scales (turbulent energy production) to the smaller scales (dissipation) is prescribed. This extended k–ε turbulence model has been rigorously benchmarked[13] with fully developed turbulent channel and pipe flows, turbulent free-shear flows, flat-plate turbulent boundary-layer flow, turbulent flow over a backward-facing step, a confined turbulent swirling flow, and dump combustor flows.[5] The

compressibility effect on the turbulence is taken into account by using the method of Mach-number correction.[16,17]

Solution Algorithm

To solve the system of nonlinear partial differential equations, finite difference approximations are used to establish a system of linearized algebraic equations on a nonstaggered grid mesh system. A pressure-based predictor plus multicorrector time marching is employed, so that flow over all speed ranges can be analyzed. The time-marching scheme and total variation diminishing (TVD) discretization are pertinent to this work and are detailed below.

Time-Marching Scheme

The time-marching scheme is described below. For convenience, transformed equation of Eq. (1) is written as

$$\frac{1}{J}\frac{\partial \rho q}{\partial t} = -\frac{\partial F_i}{\partial \xi_i} + S_q = R_q \tag{4}$$

This equation can be discretized in finite difference form:

$$\frac{1}{J\Delta t}[(\rho q)^{n+1} - (\rho q)^n] = \theta R_q^{n+1} + (1-\theta)R_q^n \tag{5}$$

where superscripts n and $n+1$ represent old and new time levels, respectively. The quantity θ is a time-marching control parameter, such that $\theta = 1.0$ and 0.5 are for a first-order implicit Euler and a second-order time-centered time-marching scheme, respectively. Second-order time accuracy is used. The following linearization is then incorporated:

$$(\rho q)^{n+1} = (\rho q)^n + \rho^n \Delta q^n \tag{6}$$

$$R_q^{n+1} = \left(\frac{\partial R_q}{\partial q}\right)^n \Delta q^n + R_q^n \tag{7}$$

With the above approximations, the final form of the time-marching scheme can be written as

$$\left[\frac{\rho^n}{J\Delta t} - \theta\left(\frac{\partial R_q}{\partial q}\right)^n\right]\Delta q^n = R_q^n \tag{8}$$

A pressure-based predictor-plus-multicorrector solution method is formulated.[7,11,12] The basic idea is to perform corrections for the pressure and velocity fields by solving for a pressure correction so that velocity–pressure coupling is enforced, based on the continuity constraint. To reduce potential oscillations in the pressure field, an upwind TVD adaptive dissipation term based on the density field, which is described in the next section, is added to the right-hand side of the pressure correction equation. The entire corrector step is repeated until the mass conservation condition is enforced before marching to the next time level.

TVD Discretization

Second-order central differencing schemes are employed to model the diffusion fluxes and the source terms of the governing equations. A third- or second-order upwind TVD scheme[12] is incorporated to model the convection terms to improve solution accuracy and to enhance numerical stability. These convection terms can be expressed by finite difference approximation as

$$\frac{\partial F}{\partial \xi} = f_{i+\frac{1}{2}} - f_{i-\frac{1}{2}} + h_{i+\frac{1}{2}} - h_{i-\frac{1}{2}} \tag{9}$$

where f and h represent first-order fluxes and TVD flux limiters, respectively. The TVD flux limiters function as antidiffusion terms to recover high-order accuracy of the scheme. The first-order fluxes and the TVD flux limiters are given below:

$$f_{i+\frac{1}{2}} = \max\left\{0, (\rho U)_{i+\frac{1}{2}}\right\} q_i + \max\left\{0, -(\rho U)_{i+\frac{1}{2}}\right\} q_{i+1} \tag{10}$$

$$h_{i+\frac{1}{2}} = \begin{cases} \frac{1}{4}|\rho U|_{i+\frac{1}{2}}\left[dq^+_{i+\frac{1}{2}} + dq^-_{i-\frac{1}{2}} + \psi\left(dq^+_{i+\frac{1}{2}} - dq^-_{i-\frac{1}{2}}\right)\right], & U > 0 \\ \frac{1}{4}|\rho U|_{i+\frac{1}{2}}\left[dq^-_{i+\frac{1}{2}} + dq^+_{i+\frac{3}{2}} + \psi\left(dq^-_{i+\frac{1}{2}} - dq^+_{i+\frac{3}{2}}\right)\right], & U < 0 \end{cases} \tag{11}$$

where the minmod functions in the TVD flux limiters are written as

$$dq^{\pm}_{i+\frac{1}{2}} = \operatorname{sign}\left(\Delta q_{i+\frac{1}{2}}\right)\max\left\{0, \min\left[\left|\Delta q_{i+\frac{1}{2}}\right|, \lambda \operatorname{sign}\left(\Delta q_{i+\frac{1}{2}}\right)\Delta q_{i+\frac{1}{2}\mp 1}\right]\right\} \tag{12}$$

The order of accuracy of this scheme is determined by the parameters ψ and λ. That is, $\lambda = (3-\psi)/(1-\psi)$, where $\psi = -1$ represents a second-order upwind TVD scheme and $\psi = \frac{1}{3}$ a third-order accurate scheme. The second-order accurate scheme is used in this study for enhanced numerical stability. The compression factor λ is used to sharpen the contact discontinuities and slipstreams for better wave-tracking resolution.

Boundary Conditions

The freestream boundary around the nozzles is modeled as a modified subsonic inlet condition regulated by a fixed total ambient pressure to allow air entrainment. This is accomplished by making two assumptions: 1) air entrainment boundaries are sufficiently far from the nozzles that the inlet freestream flow is isentropic and irrotational and 2) flow is allowed to enter through the air entrainment boundaries only. In view of assumption 1, Bernoulli's equation is used to solve for the velocity magnitude. That is, $q^n = [2(p_0 - p_e)/\rho_e]^{0.5}$, where subscript e indicates quantities extrapolated from the interior and p_0 is the ambient pressure. Obtaining a velocity magnitude q_e by extrapolation from the interior, the air speed at the entrainment boundary can be calculated as $q^{n+1} = q_e + \delta(q^n - q_e)$, where δ is a relaxation parameter. The flow directions are then extrapolated from the interior to provide smooth flow entrainment. Not to violate assumption 2, the air speed is set to zero if the flow directions indicating an outflow condition and the pressure is set to its ambient value.

The RD-170 is a regeneratively cooled, four-nozzle clustered engine fueled by kerosene and liquid oxygen and is used on Energia launch vehicles. A thermochemical analysis[1] was performed for the thrust chamber at a nominal operating condition, and the equilibrium products at the nozzle exit were used as the input to the F1 Test Stand propulsion system. $CH_{1.9423}$ was used[1] as the chemical formula for kerosene fuel. The analysis indicated that a significant amount of CO (24.569%) is present at the nozzle exit. This is the amount that could be dumped into the environment and can only be chemically reduced through afterburning. The analysis also indicated that there is no soot or polycyclic aromatic hydrocarbon fragments produced in the thrust chamber, although graphite carbon and polycyclic aromatics were considered. The lack of soot formation is to be expected, since the nominal RD-170 operating condition is a near-stoichiometric equivalence ratio of 1.2939.

Fixed water mass-flow rates are specified along the deflector wall and other wall boundaries in the flame trench. In this study, the initial water jet coming out of the flame-deflector wall was treated as a gaseous phase for computational efficiency. The enthalpy and latent heat of liquid water were lumped into the energy equation, and hence the energy change due to the vaporization of liquid water was appropriately represented. The water injection pattern is designed so that most of the water is injected at the plume impingement area. Approximately 5% of the water injects from the top wall, 10%

from each of the side walls, 15% from the top one-third of the ski slope, 40% from the middle of the ski slope, and the remaining 20% from the bottom one-third of the ski slope. Five inlet regions were specified on the ski slope to satisfy the approximate injection pattern. The freestream around the plume downstream of the trench outlet was assumed at sea-level condition with a prescribed wind speed of 10 ft/s. The initial turbulence intensities for the freestream, nozzle exit flow, and water jets were assumed at a low level of 1.5%. For the purpose of this study, that assumption is justified, since the turbulence inertia is related to the mean-flow gradients through the Boussinesq concept. When the kinetic energy term related to the normal stresses is grouped into the pressure term, the growth of the turbulence is seen to depend on the growth of the shear layers and not the initial intensity.

At exit boundaries, direct extrapolation was employed. For symmetry planes, which are the center planes of the computational domain, zero-gradient boundary conditions were applied for all scalars, and tangency conditions were imposed for the velocity vectors. Nonslip boundary conditions were employed for the momentum equations at solid-wall boundaries. Wall-normal zero-gradient pressure boundary conditions were used. Isothermal or adiabatic wall boundary conditions were specified for different wall segments, depending on the locations.

Finite-Rate Afterburning Kinetics

To accurately predict the finite-rate contaminant formations in the exhaust plume, finite-rate chemical kinetics were included in the numerical modeling. The plume chemistry occurring downstream of the nozzle exit includes the afterburning of CO, thermal NO_x formation and decomposition, and a counter-afterburning effect on CO conversion due to water quenching and its reduction effect on NO_x formation. Those chemical processes are described with a wet CO (12 reactions) and a thermal NO (6 reactions) finite-rate mechanism, as shown in Table 1. The well-known Zeldovich mechanism is included. For computational efficiency, only NO is considered in this work, since other species of the NO_x family, such as NO_2, are converted from NO and usually exist only in trace amounts. Their existence is hence included in the NO as equivalent NO. The wet CO and thermal NO mechanisms are subsets of a combustion kinetics model for complex hydrocarbon (coal-derived) fuels.[18-20] Their reaction rates, in Arrhenius-law form, have been validated with jet-stirred combustor data, including blowout limits, shock-tube measurements of ignition delay times,[19,20] and data on turbulent diffusion flames and flat flames.[21] In addition, the thermal NO_x reactions have been benchmarked using industrial burner data.[22] The simultaneous system of chemical equations is solved by using the penalty-function method.[23] The kinetic data are used to describe the plume afterburning at atmospheric pressure and not the reaction inside the high-pressure rocket combustion chamber.

Table 1 Afterburning chemical kinetics, $K_f = AT^B e^{-E/RT}$

Reaction[a]	A	B	E/R
Wet CO mechanism			
$H_2 + O_2 = OH + OH$	1.700E13	0	2.407E4
$OH + H_2 = H_2O + H$	2.190E13	0	2.590E3
$OH + OH = O + H_2O$	6.023E12	0	5.500E2
$O + H_2 = H + OH$	1.800E10	1.0	4.480E3
$H + O_2 = O + OH$	1.220E17	−0.91	8.369E3
$M + O + H = OH + M$	1.000E16	0	0
$M + O + O = O_2 + M$	2.550E18	−1.0	5.939E4
$M + H + H = H_2 + M$	5.000E15	0	0
$M + H + OH = H_2O + M$	8.400E21	−2.0	0
$CO + OH = H + CO_2$	4.000E12	0	4.030E3
$CO + O_2 = CO_2 + O$	3.000E12	0	2.500E4
$CO + O + M = CO_2 + M$	6.000E13	0	0
Thermal NO mechanism			
$O + N_2 = N + NO$	1.360E14	0	3.775E4
$N_2 + O_2 + NO + NO$	9.100E24	−2.5	6.460E4
$NO + O = O_2 + N$	1.550E9	1.0	1.945E4
$M + NO = O + N + M$	2.270E17	−0.5	7.490E4
$N + OH = NO + H$	4.000E13	0	0
$CO_2 + N = CO + NO$	2.000E11	−0.5	4.000E3

[a]M stands for a third-body collision partner.

The formation of thermal NO is significantly influenced by flame temperature. Its strong dependence on temperature results from both the temperature dependence of the forward rate constant of reaction $O + N_2 = N + NO$ and the sensitivity of the O-atom equilibrium concentration to temperature. Production of thermal NO is generally negligible at low temperatures. It is therefore expected that most of the thermal NO will be formed in the flame front, i.e., the plume mixing layer near the exit plane of the nozzles.

The coupled solution of the finite-rate kinetics with the aforementioned turbulence submodel and the governing equations of the entire CFD formulation describes adequately the effect of turbulence fluctuation on the heat release because of combustion, and vice versa. However, a different approach, which considers extra linkage between the turbulence and chemistry (herein loosely dubbed turbulence–chemistry interaction modeling), regards the preceding formulation as laminarlike and conventional, so that the extra strains in the turbulence field caused by the combustion cannot be adequately captured from it. Whether the extra linkage is necessary or not has been a continuous debate, and the topic has been investigated both theoretically and experimentally. Some excellent reviews on turbulence–chemistry interaction modeling methods can be found.[4,24] Experimentally, many conflicting observations have been made, e.g., combustion shortens the reattachment length for flame holders,[25] whereas it lengthens the recirculation zone for free wakes.[26] The real mechanisms are not well understood, and the explanations are mostly conjecture.

These conflicting observations must be addressed, however. The majority of the interaction work has been on much simpler steady-state gas-phase diffusion flames, reacting shear layers, and combustor flows, using conventional turbulence models that do not produce acceptable results. However, it is entirely possible that whatever discrepancies may have occurred have little to do with the conventional turbulence formulation, but are caused by the numerical algorithms, boundary conditions, thermodynamics, kinetics models, and turbulence models. Indeed, many sophisticated turbulence models cannot generate good results even for nonreacting flows.[15]

Another important aspect often ignored by many investigators is that the experiment must be designed and conducted to provide sufficient information on the boundary conditions (inlet conditions in particular) to allow for reconstruction of the flowfield if the data are to be of value in turbulent-combustion-model development and evaluation.[27] Models based on experiments without adequate boundary conditions are not very helpful. A turbulence–chemistry interaction model can hence be viewed as a special form of turbulence modeling attempting to locate the extra linkage in the combustion-driven flow physics. Earlier models such as the eddy-breakup[28] model are too limited to describe most diffusion flames of practical fuels.[24]

Recent development has centered around the probability density function (PDF) methods such as the computed PDF and the assumed PDF methods. A Monte Carlo PDF reactor model has been applied by one of the authors to study the unmixedness in a jet-stirred combustor.[20] Such a model, if combined with a flowfield solution, is very similar to a computed PDF method.[29] The computed PDF method, however, is judged[30] not suitable for supersonic combustion. In addition, the computational effort is so expensive at present that the method is not a useful engineering tool.[30]

In assumed PDF methods, care should be taken in interpreting results from theoretical studies, because the implications cannot be substantiated and often are contradictory to experimental observations, especially those modeled on the mixing effect only[31] or the chemistry effect only,[32] since only part of the turbulence–chemistry interaction is described.

A recent benchmark effort,[30] in which a multivariate Beta PDF linked for mixing and a joint PDF linked for chemistry are explored, is probably a typical representative among the state-of-the-art assumed PDF methods. Although the means and sums of variances for species were provided from the expriment, the result showed that the assumed PDFs give adequate agreement only in regions where combustion has not taken place; in all other situations, the agreement is inadequate. The mean temperature profiles computed with

the PDF showed marginal improvement over those without the PDF. The solution was insensitive to the initial turbulent intensity (which reconfirms our assumption that inlet intensity has minor effect on the eventual turbulence level). In addition, better agreement is seen when the chemical source term is turned off. The outcome of this benchmark effort reinforces the notion that if state-of-the-art PDFs cannot properly describe the turbulence–chemistry interaction for a simple experiment, with the means and variances for species given, the PDF method is not ready for the study of complex test-stand flow physics. Furthermore, the problems in modeling the Favre-averaged correlations using approximations developed for the corresponding Reynolds-averaged terms and/or the use of the incompressible form of the turbulent kinetic energy equation will, if not resolved, forever produce discrepancies for PDF methods.

On the other hand, a recent study[15] found the conventional laminarlike treatments performed as well as or better than the computed PDF method for a turbulent reacting compressible shear layer. The computed PDF method predicted erroneous ignition delay and flame thickness. The contention that the conventional methods cannot adequately capture the extra strains in the turbulence field caused by the combustion seems to be unfounded, at least for the current flows of interest.

In veiw of the above discussion and the need for computational tractability in an engineering tool, the computationally efficient conventional method is preferred in this study.

Computational Grid Generation

The F1 Test Stand at MSFC, standing 230 ft tall with a flame bucket (deflector) attached to the aspirator, was used to test the F1 engines that propelled the Saturn launch vehicles. Not only does the flame bucket quench the rocket exhaust plume with deluge water jets, but it also turns the vertically flowing exhaust plume into a horizontal direction, after which the plume expands and dissipates into the atmosphere. Figure 1 shows the computational domain for the F1 Test Stand. The RD-170 engine is mounted vertically, firing downward into the flame bucket. Because of the symmetry, only half of the domain was actually computed. The four RD-170 nozzles (mounted beneath a platform that is not modeled) and the aspirator are described by zone 1, which contains 63,360 grid points (72 × 40 × 22). The aspirator itself is mounted on top of the flame bucket so that the air entrainment is promoted and the plumes are centered while impinging on a predetermined area in the flame bucket (approximately 45-deg elbow at the bottom). Ambient air is allowed to be entrained through the top and four side boundaries of

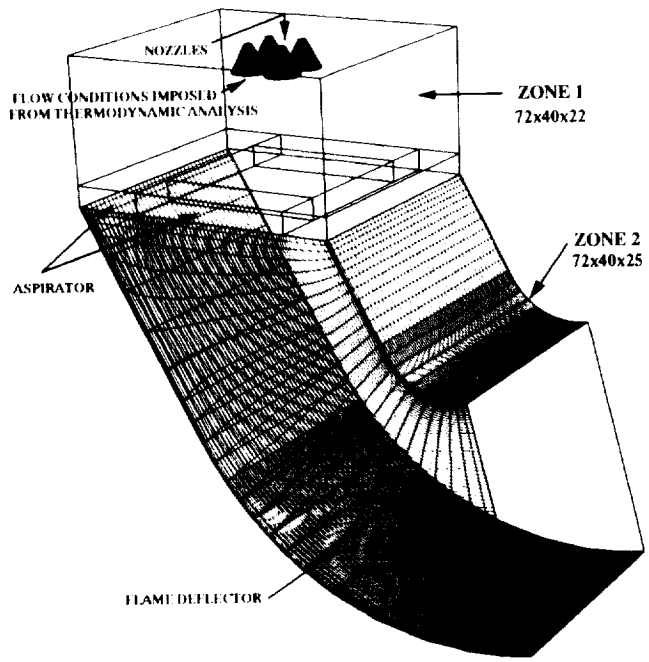

Fig. 1 Computational domain for the RD-170 nozzles and F1 Test Stand.

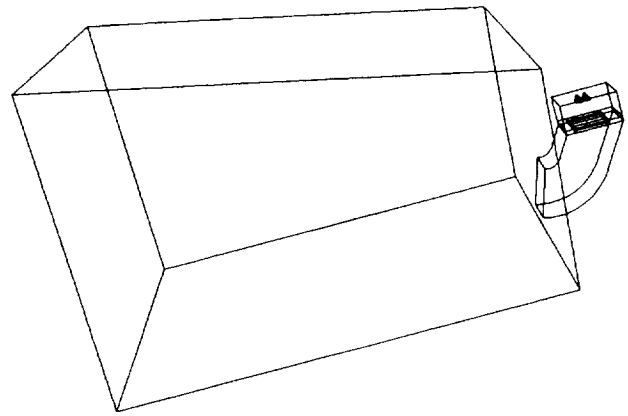

Fig. 2 Computational domain for all three zones.

zone 1. The flame bucket is modeled by zone 2, which comprises 72,000 grid points (72 × 40 × 25). The deflector-restricted plumes are quenched through water deluge injecting from all four walls inside the bucket. After passing through the flame bucket (zone 2), the quenched plumes expand into the surrounding atmosphere (zone 3), which is described by 156,975 grid points (91 × 69 × 25). The relative sizes and locations of all three zones are shown in Fig. 2. The total number of grid points used in this study was 292,335. The computational grid was generated using the EZSURF code.[33] The edge curves of the nozzle exits, aspirator, flame deflector, and multizone block edges were generated first. Transfinite interpolation was applied to create the initial surfaces. The flame deflector and nozzle exit surfaces were elliptically smoothed using Bezier-curve and local redistribution techniques. The volume grid for the first block (zone 1) was created using two linear stackings: one from the top of the block to the nozzle exit plane and then another from the nozzle exit plane to the bottom of the aspirator. The flame deflector block (zone 2) and subsequent external ambience (zone 3) volume grids were created using transfinite interpolation.

Results and Discussion

Figure 3 shows the computed temperature contours for the water-quenching case at selected computational planes. Water-jet vectors are shown for the top and bottom walls. The water jets at the back wall are shown, but are mostly blocked out by the temperature contours, whereas the water jets from the front wall are omitted for clarity. The plumes impinge on the 45-deg bend section of the flame bucket, where they encounter the most water deluge. This impingement location agrees with the original test-stand design. The quenched plumes then turn and partly hit the outer wall, where they move horizontally, following the direction of the flame bucket. Most of the computed thermal NO is formed near the aspirator region of the flowfield, where significant mixing and the highest temperature occur. The coincidence of high temperature and NO formation is in agreement with the characteristics of the Zeldovich mechanism.

Figure 4 shows comparisons of averaged mass fraction in the system for species CO, CO_2, NO, and OH with respect to the elapsed time. The averaged mass fraction for CO in the nominal case is more than that for the purely finite-rate chemistry case because of the counter-afterburning effect of deluge water, and vice versa for that of CO_2. The higher level of OH in the finite-rate case shows a higher degree of afterburning reaction, due to the higher overall plume temperature without water quenching. Total NO production drops significantly in the nominal case. The concentration of NO in the nominal case is almost two orders of magnitude lower than that in the case of finite-rate chemistry only. The low emission of NO in the water-quenching case is not surprising, since the extent of thermal NO formation depends heavily on the local temperature. The effect of water deluge on the formation of NO is due to the reduction in peak plume temperature.

The computed growth of plume volumes is shown in Fig. 5. Note that the growth rates of the plumes have reached their approximate asymptotic states. Obviously, the plume energy of the finite-rate chemistry case is higher than that of the nominal case.

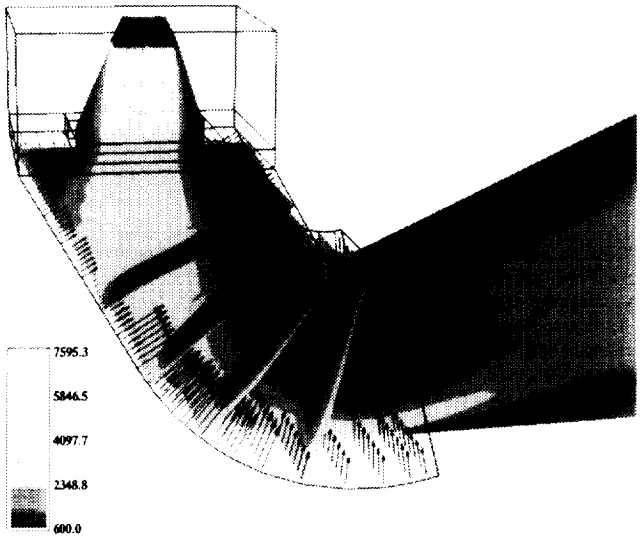

Fig. 3 Computed temperature contours for the nominal case.

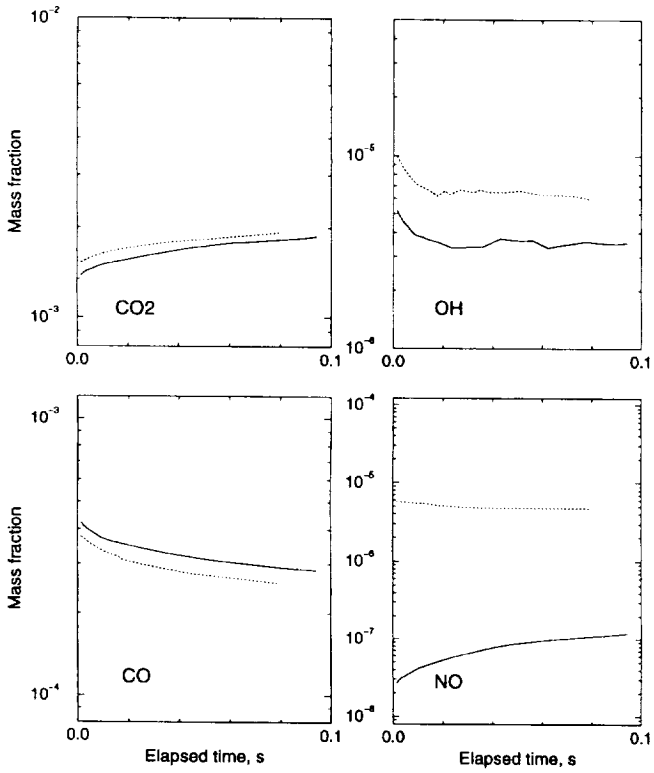

Fig. 4 Comparisons of averaged mass fraction in the system for species CO, CO_2, NO, and OH: ·····, finite-rate chemistry case and ——, nominal case.

Correspondingly, the plume volume growth rate of the finite-rate case is larger than that of the nominal case. It is anticipated that the characteristics of computed growth of plume energies would be similar to those of plume volumes. These CFD results ultimately serve as the basis (input) for a subsequent meteorological cloud dispersion calculation, where the plume volume growth rate helps determine the eventual plume size, and the plume energy growth rate helps determine the magnitude of the plume buoyancy force.

A comparison of the calculated criterion pollutant total emission rates for RD-170 with those measured for other engines[34] is shown in Table 2. MA5B and MA3B are booster engines, and MA3S is a sustainer engine. The plume characteristics of RS27 is similar to those of the booster engines. Although the engine types are different, those engines are similar to RD-170 in that all burn kerosene and liquid oxygen. In addition, all were vertically mounted and firing

Table 2 Total emission rates

Engine	Thrust, lbf	Rate, lb/s NO_x	Rate, lb/s CO
RD-170, CFD, frozen	1,777,000	——	1382
RD-170, CFD, finite rate	1,777,000	8.0	232
RD-170, CFD, nominal	1,777,000	0.4	463
MA5B, hot firing	370,000	5.4/25.9[a]	133/641[a]
MA3S, hot firing	165,000	2.7/29.1[a]	210/2266[a]
MA3B, hot firing	60,000	1.5/45.6[a]	38/4111[a]
RS27, hot firing	205,000	1.2/10.6[a]	94/820[a]

[a]Based on extrapolation of measured emission rate to an RD-170 by thrust ratio.

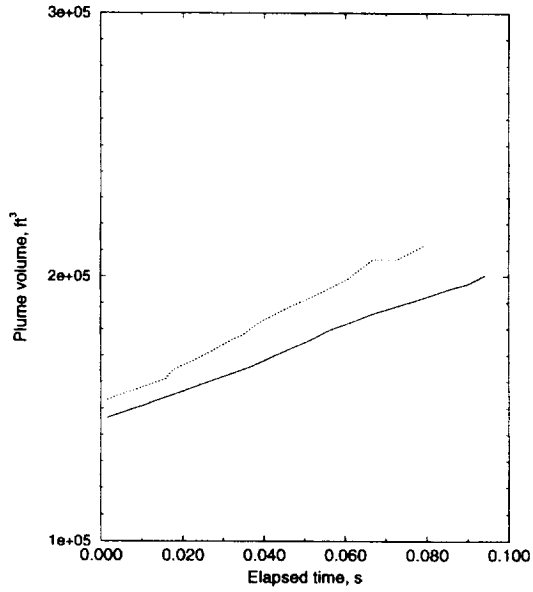

Fig. 5 Comparison of plume volume growth: ·····, finite-rate chemistry case and ——, nominal case.

down into to a bucket. The bucket, similar to that of the F1 Test Stand, is also a 45-deg deflector, and the backwall of the bucket is also perforated to allow water deluge. Since thrust levels are different for those engines, the measured emission rates and those extrapolated to an RD-170 level by thrust ratios are both shown. Note that the emission rates for those engines are based on sampling of actual firings, analyses of fuel samples, and engineering extrapolations. The computed emission growth is based on integrating the species concentration over the entire plume boundary and in theory is more accurate than extrapolation from several sampling points to infer the whole plume. Nevertheless, the comparison is instructive, and the agreement in order of magnitude is encouraging. The predicted CO and NO_x total emission rates for RD-170 testing on the F1 Test Stand, from finite-rate chemistry to nominal water deluge, are less than those of other hydrocarbon-engine tests when compared at same thrust level. Comparing the predicted RD-170 emission rates with those of other engines at their original measured values, the finite-rate and nominal cases have values comparable with those of tests. The high CO emission rate and zero NO emission of the frozen-chemistry case are to be expected, because afterburning and thermal NO reactions were not considered. In the finite-rate case, the NO emission rate increases to 8 lb/s while the CO emission rate drops to 232 lb/s, apparently caused by the unabated afterburning of CO and thermal NO creation from N_2 without water quenching. At nominal F1 Test Stand operating conditions, because of the plume quenching, the reduction of CO emission and the production of NO emission are decreased. Although the thrust of RD-170 is higher than those of the other hydrocarbon engines, the NO_x emission rate of its nominal firing on the F1 Test Stand is lower than those of the other engines, whereas its CO emission rate is higher than those of the other engines, which may be explained by the higher water deluge capacity of the F1 Test Stand (about 100,000 gal/min) and the lower capacity (10,000–15,000 gal/min) of the other test stands.[34] This comparison indicates that one of the controlling parameters for

the emission rates of the two chemically counterproducing criterion pollutants is the test-stand quenching capacity.

Conclusion

An asymptotic plume growth method based on a three-dimensional CFD formulation has been developed to predict the contaminant emissions from simulated ground-based RD-170 engine hot-fire testing. Pertinent test-stand flow physics, such as the interaction between the multiple-nozzle clustered engine and the plume, aspiration from base and aspirator, plume mixing with entrained air that resulted in contaminant dilution and afterburning, counter-afterburning due to flame-bucket water quenching, plume impingement on the flame bucket, and restricted multiple-plume expansion and turning, has been predicted. The emission levels of the criterion pollutants are controlled by the plume temperature and the test-stand quenching capacity. The predicted criterion pollutant total emission rates agreed reasonably well with those of the existing hydrocarbon engine hot-firing test data.

Acknowledgments

The authors are thankful for the support from Robert Schwinghamer of the NASA Operational Environment Team. The discussions with Rebecca McCaleb and Clay Horan of the Environmental and Engineering Office are also appreciated. We would also like to thank Denise Doran of MSFC and Catherine Dumas of Sverdrup for preparing the contour graphics.

References

[1]Svehla, R. A., and McBride, B. J., "FORTRAN IV Computer Program for Calculation of Thermodynamic and Transport Properties of Complex Chemical Systems," NASA TN D-7056, Jan. 1973.

[2]Leone, D. M., and Turns, S. R., "Active Chlorine and Nitric Oxide Formation from Chemical Rocket Plume Afterburning," AIAA Paper 94-0788, Jan. 1994.

[3]Wang, T.-S., and McConnaughey, H. V., "Two-Dimensional Flame Trench Simulation During Engine Shut Off," NASA/MSFC, 4th SSME CFD Workshop Meeting, Huntsville, AL, April 1986.

[4]Correa, S. W., and Shyy, W., "Computational Models and Methods for Continuous Gaseous Turbulent Combustions," *Progress in Energy and Combustion Science*, Vol. 13, No. 1, 1987, pp. 249–292.

[5]Wang, T.-S., Chen, Y.-S., and Farmer, R. C., "Numerical Study of Reactive Ramjet Dump Combustor Flowfield with a Pressure Based CFD Method," AIAA Paper 89-2798, July 1989.

[6]Wang, T.-S., and Luong, V., "Hot-Gas-Side and Coolant-Side Heat Transfer in Liquid Rocket Engine Combustors," *Journal of Thermophysics and Heat Transfer*, Vol. 8, No. 3, 1994, pp. 524–530.

[7]Wang, T.-S., and Chen, Y.-S., "Unified Navier–Stokes Flowfield and Performance Analysis of Liquid Rocket Engines," *Journal of Propulsion and Power*, Vol. 9, No. 5, 1993, pp. 678–685.

[8]Wang, T.-S., Chen, Y.-S., Farmer, R. C., and Tucker, P. K., "Numerical Investigation of the Transient SSME Fuel Preburner Combustor Flowfield," AIAA Paper 90-0646, Jan. 1990.

[9]Wang, T.-S., "Numerical Study of the Transient Nozzle Flow Separation of Liquid Rocket Engines," *Computational Fluid Dynamics Journal*, Vol. 1, No. 3, 1992, pp. 319–328.

[10]Wang, T.-S., "Numerical Analysis of Base Flowfield for a Four-Engine Clustered Nozzle Configuration," *Journal of Propulsion and Power*, Vol. 11, No. 5, 1995, pp. 1076–1078.

[11]Chen, Y.-S., "Compressible and Incompressible Flow Computations with a Pressure Based Method," AIAA Paper 89-0286, Jan. 1989.

[12]Chen, Y.-S., Liaw, P., Shang, H.-M., and Chen, C.-P., "Numerical Analysis of Complex Internal and External Viscous Flows with a Second-Order Pressure-Based Method," AIAA Paper 93-2966, July 1993.

[13]Chen, Y.-S., and Kim, S. W., "Computation of Turbulent Flows Using an Extended k–ε Turbulence Closure Model," NASA CR-179204, Oct. 1987.

[14]Launder, B. E., and Spalding, D. B., "The Numerical Computation of Turbulent Flows," *Computer Methods in Applied Mechanics and Engineering*, Vol. 3, No. 2, 1974, pp. 269–289.

[15]Kim, S.-W., "Numerical Investigation of Chemical–Turbulence Interaction in Compressible Shear Layers," *Combustion and Flame*, Vol. 101, 1995, pp. 197–208.

[16]Chen, Y.-S., Cheng, G.-C., and Farmer, R. C., "Reacting and Non-Reacting Flow Simulation for Film Cooling in 2-D Supersonic Flows," AIAA Paper 93-3602, July 1992.

[17]Cheng, G.-C., Farmer, R. C., and Chen, Y.-S., "Numerical Study of Turbulent Flows with Compressibility Effects and Chemical Reactions," AIAA Paper 94-2026, June 1994.

[18]Edelman, R. B., Farmer, R. C., and Wang, T.-S., "Combustion and Emissions of Synthetic Fuel Components—Analysis and Modeling," *Combustion of Synthetic Fuels*, edited by W. Bartok, American Chemical Society Symposium Series 217, 1983, pp. 29–48.

[19]Wang, T.-S., Farmer, R. C., and Tucker, P. K., "Turbulent Hydrocarbon Combustion Kinetics—Stochastic Modeling and Verification," AIAA Paper 89-0486, Jan. 1989.

[20]Wang, T.-S., Farmer, R. C., and Edelman, R. B., "Turbulent Combustion Kinetics for Complex Hydrocarbon Fuels," AIAA Paper 88-0733, Jan. 1988.

[21]Edelman, R. B., and Harsha, P. T., "Some Observations on Turbulent Mixing with Chemical Reactions," *Turbulent Combustion*, edited by L. A. Kennedy, Vol. 58, Progress in Astronautics and Aeronautics, AIAA, New York, 1978, pp. 55–101.

[22]Harsha, P. T., Edelman, R. B., Wang, T.-S., and Farmer, R. C., "Performance Modeling of Advanced Gas Burner Systems," GRI-82/0016, Science Applications, Inc., SAI 82-041-CHA, Chatsworth, CA, June 1982.

[23]Chen, Y.-S., and Farmer, R. C., "Computations of Premixed and Diffusion Flames with a Fast Chemistry Integration Scheme," *4th International Symposium on CFD*, Univ. of California at Davis, CA, 1991, pp. 172–177.

[24]Bilger, R. W., "Turbulent Diffusion Flames," *Annual Review of Fluid Mechanics*, Vol. 21, 1989, pp. 101–135.

[25]Pitz, R. W., and Daily, J. W., "Combustion in a Turbulent Mixing Layer Formed at a Rearward-Facing Step," *AIAA Journal*, Vol. 21, No. 11, 1983, pp. 1565–1570.

[26]Winterfeld, G., "On Processes of Turbulent Exchange Behind Flame Holders," *10th Symposium (International) on Combustion*, Combustion Inst., 1965, pp. 1265–1275.

[27]Dandekar, K. V., and Gouldin, K. V., "Temperature and Velocity Measurements in Premixed Turbulent Flames," *AIAA Journal*, Vol. 20, No. 5, 1982, pp. 652–659.

[28]Spalding, D. B., "Mixing and Chemical Reaction in Steady Confined Turbulent Flame," *13th Symposium (International) on Combustion*, Combustion Inst., 1970, pp. 649–658.

[29]Pope, S. B., "PDF Methods for Turbulent Reacting Flows," *Progress in Energy and Combustion Science*, Vol. 11, No. 1, 1985, pp. 119–192.

[30]Baurle, R. A., Alexopoulos, G. A., and Hassan, H. A., "Assumed Joint Probability Density Function Approach for Supersonic Turbulent Combustion," *Journal of Propulsion and Power*, Vol. 10, No. 4, 1994, pp. 473–484.

[31]Peng, X., "Sensitivity Study of the Effects of PDF Models on the Predicted Structure of Turbulent Combustion Flows," M.S. Thesis, Dept. of Mechanical Engineering, Univ. of Tennessee, Knoxville, TN, 1988.

[32]Gaffney, R. L., White, J. A., Girimaji, S. S., and Drummond, J. P., "Modeling Turbulent/Chemistry Interactions Using Assumed PDF Methods," AIAA Paper 92-3638, July 1992.

[33]Warsi, S., "Algebraic Surface Grid Generation in Three-Dimensional Space," NASA CP-3143, April 1992.

[34]Anon., "Estimation of Pollutants in Rocket Exhaust," Rockwell International, Final Rept., EMSC8035.7FR(2), May 1984.

I. D. Boyd
Associate Editor